The Trans-Pacific Transport of Dust in 2007 - a MODIS/CALIOP Study

by

LU WANG

A Dissertation submitted to the

Graduate School-Newark

Rutgers, The State University of New Jersey

in partial fulfillment of the requirements

for the degree of

Master of Science

Graduate Program in

Environmental Sciences

written under the direction of

Dr. Yuan Gao

and approved by

_____

_____

_____

_____

Newark, New Jersey

May, 2012

ABSTRACT OF THE DISSERTATION

The Trans-Pacific Transport of Dust in 2007 - a MODIS/CALIOP Study

By LU WANG

Dissertation Director:

Dr. Yuan Gao

Asian dust transported to the west coast of the United States and Canada has an impact on the local air quality. Thus, it is important to investigate the trans-Pacific transport of dust. In this study, observations from two satellite instruments in 2007 were utilized to evaluate this eastward flux of Asian dust – the 550 nm column aerosol optical depth and fine-mode fraction from the Moderate Resolution Imaging Spectroradiometer (MODIS), and the 532 nm column aerosol optical depth and volume depolarization ratio from the Cloud-Aerosol LIdar with Orthogonal Polarization (CALIOP). The satellite observations were then compared with the Geophysical Fluid Dynamics Laboratory Global Chemical Transport Model (GCTM) simulations.

In both satellite studies, the eastward flux of dust displayed distinct meridional variations on both sides of the North Pacific, peaking between 30 and 40°N in the NW Pacific and between 40 and 50°N in the NE Pacific. Both MODIS and CALIOP revealed the same seasonal pattern of the eastward dust flux in 2007: maximum in spring, minimum in summer, relatively high in winter, and intermediate in fall between that in summer and winter. Despite large discrepancies in magnitude, the percentages of the seasonal contributions to the annual dust fluxes agreed well between the MODIS and CALIOP estimates. This satellite-observed seasonal pattern was different from that simulated by GCTM. Though also having the spring maximum, GCTM showed comparable dust fluxes in winter and fall which were both significantly lower than that in summer. The annual efficiency of the eastward dust transport was 64% as estimated by MODIS and 22% by CALIOP. Both approaches indicated seasonal variations in transport efficiencies with high efficiency observed in winter. In contrast, GCTM simulated relatively constant transport efficiencies throughout the year, averaged 13% for 2007. Overall, MODIS estimated greater dust fluxes than CALIOP, by about 5-fold for the NW Pacific and 14-fold for the NE Pacific. GCTM simulated even lower dust fluxes than CALIOP.

Acknowledgements

I would like to thank Dr. Yuan Gao as my thesis advisor. I also thank Dr. Evert Jan Elzinga and Dr. Adam Kustka who are my dissertation members.

I am much obliged to Ms. Liz Morrin, Dr. Alex Gates, and Dr. Lee Slater for their great departmental support.

I am sincerely thankful to Dr. Songmiao Fan and Dr. Bud Moxim for their GCTM simulation results and their valuable comments and discussions on this thesis work; to Dr. Paul Ginoux for the enlightening conversation on Asian dust transport height determination; to Dr. Didier Tanré, Dr. Hongbin Yu, and Dr. Robert Levy for their great help in MODIS data processing; to Dr. Zhaoyan Liu and Dr. Ritesh Gautam for their great help in CALIOP data processing; to Dr. James Anderson for his valuable comments on Asian dust; and to Dr. Jim Miller for his readiness to help.

I feel especially grateful to Lili Xia, Sweeta Chauhan, Chi Zhang, and Jiping "Jeannie" Wang for their invaluable help during my extremely difficult times. I also thank Joshua Lefkowitz, Ying Zhu, Mike Kalczynski, and Mehrez Elwaseif for their help. I am thankful to Dawn Semple, Nathi Kijpatanasilp, James Nolan, my roommates and others for being pleasant companions during this short journey of my life.

TABLE OF CONTENTS

List of Tables

List of Figures

List of Abbreviations and Symbols Used

Abbreviation/Symbol	Notation
AI	Aerosol index
AOD	Aerosol optical depth
AOD_{du}	Dust aerosol optical depth
$AOD_{du,\ in}$	Annual average of dust aerosol optical depth in the North America inflow region
$AOD_{du,out}$	Annual average of dust aerosol optical depth in the East Asia outflow region
$(AOD_{du}/AOD)_{in}$	Ratio of annually averaged dust aerosol optical depth to annually averaged total aerosol optical depth in the North America inflow region
$(AOD_{du}/AOD)_{out}$	Ratio of annually averaged dust aerosol optical depth to annually averaged total aerosol optical depth in the East Asia outflow region
$AOD_{du,in}/AOD_{du,out}$	Ratio of annually averaged dust aerosol optical depth in the North America inflow region to that in the East Asia outflow region
AOD_{in}	Annual averaged column aerosol optical depth in the North America outflow region
AOD_{m}	Marine aerosol optical depth
AOD_{out}	Annual averaged column aerosol optical depth in the East Asia inflow region
AQPMS	Air Quality Prediction Modelling System
AVHRR	Advanced Very High Resolution Radiometer
CALIOP	Cloud-Aerosol LIdar with Orthogonal Polarization
CALIPSO	Cloud-Aerosol Lidar and Infrared Pathfinder Satellite Observations
EOS	Earth Observing System
f	Fine-mode fraction
f_a	Fine-mode fraction of anthropogenic pollution
f_d	Fine-mode fraction of dust
f_m	Fine-mode fraction of marine aerosol
F_{du}	Flux of dust (Tg)
GFDL	Geophysical Fluid Dynamics Laboratory
GCTM	Global Chemical Transport Model
GOCART	Georgia Tech/Goddard Global Ozone Chemistry Aerosol Radiation and Transport
HNLC	High Nutrient – Low Chlorophyll
L	Longitudinal length (m)

M_{du}	Mass concentration of dust (g/m^2)
MODIS	Moderate Resolution Imaging Spectroradiometer
OMI	Ozone Monitoring Instrument
TOMS	Total Ozone Mapping Spectrometer
u	u-wind (m/s)
UV	ultra-violet
VDR	Volume depolarization ratio
w	Surface wind (m/s)

当时只道是寻常

— 清 • 纳兰性德 (Nalan Xingde, 1655-1685)

Chapter 1: Introduction

Dust is an important tropospheric aerosol species. It can directly affect the climate by scattering and absorbing solar radiation and Earth's thermal radiation and then altering the aerosol radiative forcing [Haywood & Boucher, 2000; Denman *et al*., 2007; Forster *et al*., 2007]. By influencing cloud microphysical properties and cloud lifetime, dust can modulate precipitation processes and thus have an indirect effect on the climate [Huang *et al*., 2009; Kaufman *et al*., 2005a; Li & Min, 2010; Zhang *et al*., 2009, Rosenfeld *et al*., 2001]. Elevated by winds from its sources in dried or semi-dried regions, dust can travel over long distance and eventually return to the Earth's surface by dry or wet deposition. Dust deposited into the ocean brings continental minerals (such as Fe) to the water, which can feed the local phytoplankton communities. The Fe influxes into water due to atmospheric dust deposition are especially critical for those oceanic regions where the biomass is limited by the availability of Fe (e.g. the High Nutrient – Low Chlorophyll (HNLC) regions) [Martin, 1990; Jickells *et al*., 2005].

East Asia is one of the largest sources of dust in the world. The major source regions of Asian dust are the Gobi Desert of Inner Mongolia and the Taklimakan Desert in China [Sun *et al*., 2001; Wang *et al*., 2004]. Dust from these two regions follow different transport pathways: the Gobi dust is usually entrained to 2-3 km high and deposits mainly in the Loess Plateau, southeastern China, offshore, and near Pacific regions; in contrast, the Taklimakan dust can be elevated to a much higher altitude (4-7 km) and travel over a much longer distance across the ocean, serving as a source of aeolian sediments in the remote North Pacific [Kwon *et al*., 1997; Sun *et al*., 2001; Huang *et al*., 2008]. It has long been

observed that the Asian dust can be transported across the North Pacific to the west coast of the United States or Canada [Jeffe *et al*., 1999; Husar *et al*., 2001; McKendry *et al*., 2001].

The transpacific transport of Asian dust and its deposition along the way has been studied over decades [Uematsu *et al*., 1983; Duce *et al*., 1991; Jeffe *et al*., 1999; Gao *et al*., 2001; Husar *et al*., 2001; Chin *et al*., 2003; Gao *et al*., 2003; Uematsu *et al*., 2003; Huang *et al*., 2008; Hsu *et al*., 2009]. In general, these studies use three approaches – the ground-truth measurement, model simulation, and remote-sensing approach.

The ground-truth approach directly measures the flux of particulate matter with size fractions in the range of dust particles. Most commonly, the concentration of particulate aluminum (Al), a representative crustal element, in air or marine sediment samples is measured first. Then, by using a weight percentage of 6-8% for Al in dust [Duce *et al*., 1980], the measured Al concentration is converted to the dust concentration. The corresponding dry and wet deposition rates of dust are computed using representative values of dry deposition velocity of dust, scavenging ratio by rain and meteorological precipitation data. Direct measurements are usually conducted at long-term observation stations or at sea during cruises. Using this approach, Gao *et al*. (1997) obtained the off-shore total fluxes of dust 26 g m^{-2} yr^{-1} in the East China Sea and 10 g m^{-2} yr^{-1} in the South China Sea, which corresponded to an annual total dust deposition in the off-shore China Sea about 63 Tg in 1992. Hsu *et al*. (2009) estimated an average dust flux of ~ 20 g m^{-2} yr^{-1} for the East China Sea, contributing to ~18 Tg annual dust deposition into this area for the period between February 2002 to February 2007. Based on their sediment trap

measurements in September 1984, Masuzawa *et al*. (1989) estimated a dust deposition rate of 6.0-12 g m^{-2} yr^{-1} for the Japan Sea. For the remote central North Pacific, Uematsu *et al*. (1983) estimated a dust deposition rate of 6-12 Tg yr^{-1}, by synthesizing their observations (with two-week sampling interval) at four representative stations during January 1981 and March 1982. Using an improved scavenging ratio for dust, Uematsu *et al*. (1985) re-examined the above observations and derived a new deposition rate of ~20 Tg yr^{-1} for the central North Pacific, which was almost 2-fold of their previous estimate. Duce *et al*. (1991) estimated a dust flux into the entire North Pacific of 5.3 g m^{-2} yr^{-1}, corresponding to an annual deposition of 480 Tg dust. Although for a specific study site, ground-truth dust measurements are of most accurate compared with model simulation and remote-sensing observations, their temporal and spatial coverage is extremely limited. For large-scale studies, data extrapolation often has to be performed, which brings great uncertainties in dust flux estimation.

Dust transport and deposition in the North Pacific has been simulated by a number of models. On their first attempt, researchers developed simple models to estimate the dry and wet deposition of dust at stations and extrapolated the estimation to a vast region [Duce & Tindale, 2001; Jickells & Spokes, 2001]. Using this approach, Gao *et al*. (2001) obtained an annual atmospheric iron deposition of 3 Tg into the North Pacific due to the aeolian dust transport from Asia. By assuming 3.5% fraction of iron in the dust [Taylor & McLennan, 1985], this iron input can be converted to an annual dust deposition of 85 Tg into the North Pacific. Gao *et al*. (2001) also computed the seasonal deposition rates of iron for this region, which were corresponding to dust deposition rates of 8 Tg $month^{-1}$ in

spring, 5 Tg $month^{-1}$ in summer, 10 Tg $month^{-1}$ in fall, and 6 Tg $month^{-1}$ in winter. Current dust models are more sophisticated. In the context of simulated meteorological fields, these models take into account of the distribution of dust source regions, dust particle size distribution, the advection, convection, boundary layer mixing, dry deposition, and wet scavenging of dust during transport. The simulated dust concentrations and dust fluxes are placed in evenly-spaced grids over the lands and oceans. The Geophysical Fluid Dynamics Laboratory Global Chemical Transport Model (GFDL-GCTM) serves for this purpose. Gao *et al*. (2003) used it to simulate the input of dust-derived dissolved Fe into the North Pacific. The estimated wet and dry deposition of dissolved Fe ranged from 0.12 to 0.89 Tg yr^{-1} and 0.018 to 0.071 Tg yr^{-1} respectively, accounting for 4-30% and 0.6-2.4% of the total dust Fe fluxes into this area. Utilizing the Georgia Tech/Goddard Global Ozone Chemistry Aerosol Radiation and Transport (GOCART) model, Chin *et al*. (2003) successfully simulated the dust evolution and its transpacific transport during the ACE-Asia 2001 experiment. Using a regional model - Air Quality Prediction Modelling System (AQPMS), Uematsu *et al*. (2003) simulated a 1-year (March 1994-February 1995) Asian dust deposition for the North Pacific. Their results suggested an annual dust flux of 2.7 g m^{-2} yr^{-1} from East Asia, corresponding to an annual input of 64 Tg dust for the Northwest Pacific region. Nonetheless, there are large discrepancies between the dust fluxes simulated by different numerical models, mainly due to insufficient understanding of the dust emission, transport, and deposition processes. For this reason, it is essentially important to validate the dust models with field observations.

Satellites have wide temporal and spatial coverage. Some unique physical and chemical properties of dust enable its detection by remote sensors. In recent decades, remote-sensing techniques have been increasingly used to investigate the atmospheric dust distribution and long-range transport [Carlson, 1979; Husar *et al*., 2001; Prospero *et al*., 2002; Ginoux & Torres, 2003; Kaufman *et al*., 2005b; Gassó & Stein, 2007; Huang *et al*., 2008; Liu *et al*., 2008; Gautam *et al*., 2009; Yu *et al*., 2010]. The pioneering remote-sensing studies on dust used satellite aerosol optical depth (AOD) observed by the Advanced Very High Resolution Radiometer (AVHRR) [Prospero & Carlson, 1972; Prospero & Nees, 1977; Carlson 1979]. Not designed for aerosol observation, AVHRR cannot distinguish dust from other types of tropospheric aerosols, such as pollutant, sea salt, and smoke. Later, the Total Ozone Mapping Spectrometer (TOMS) was used based on the ultra-violet (UV) absorption property of dust [Herman *et al*., 1997; Ginoux & Torres, 2003]. TOMS can differentiate dust and smoke from pollutant and sea salt. Its modern successor is the Ozone Monitoring Instrument (OMI) onboard the NASA's Earth Observing System (EOS) Aura. Gassó & Stein (2007) used the aerosol index (AI) product of OMI to study dust in the sub-Antarctic region. The daily AI image from OMI has become a good tool to study the evolution of dust.

A milestone remote-sensing study on dust was conducted by Kaufman *et al*. (2005b). In their study, an algorithm was developed based on the columnar AOD and fine-mode fraction retrievals from the Moderate Resolution Imaging Spectroradiometer (MODIS) instrument. This aerosol algorithm allowed people to partition the observed total columnar AOD into three parts, attributing to dust, anthropogenic pollution and sea salt,

respectively. The MODIS instruments onboard the Terra and Aqua satellites have made near daily observations of atmospheric aerosols since February 24, 2000 (Terra) and July 03, 2002 (Aqua). Currently, it has become one of the most popular satellite instruments for researcher to study the large-scale distribution and transport of dust and pollution aerosols.

Another important advance in remote-sensing study on dust is associated with the operation of the Cloud-Aerosol LIdar with Orthogonal Polarization (CALIOP) onboard the Cloud-Aerosol Lidar and Infrared Pathfinder Satellite Observations (CALIPSO) satellite. CALIPSO started to provide data for cloud and aerosol studies since June 7, 2006. Unlike previous passive sensors which can acquire only columnar aerosol properties, CALIOP can provide profile information on aerosol type and aerosol optical extinction throughout a certain vertical air column [Winker *et al*., 2003; Liu *et al*., 2008; Winker *et al*., 2009]. Using the 532 nm total attenuated backscatter intensity, volume depolarization ratio (VDR), and 1064 nm/532 nm backscatter color ratio records from CALIOP, Huang *et al*. (2008) studied the vertical distribution and transport path of dust during a couple major dust events in China in 2007. Based on the AOD and VDR records from CALIOP Layer product, Gautam *et al*. (2009) revealed different tropospheric dust loading over India during the two pre-monsoon seasons of 2007 and 2008. Yu *et al*. (2010) compared the cloud-free AOD at 532 nm observed by CALIOP with GOCART simulations and MODIS retrievals at 550 nm. They found that these three sets of AOD had large discrepancies in magnitude, but generally showing similar geographic patterns and seasonal variations. For the NW Pacific, they found that the CALIPSO AOD tended

to bias low, possibly stemming from misclassification of aerosols transported to the upper troposphere as thin cirrus clouds and missing of heavy aerosol loading events due to the long time interval between CALIPSO repeating visits (~ 16 days compared with MODIS near daily cycle). The authors also noticed that in the NW Pacific MODIS easily suffered from cloud contamination and tended to bias AOD high.

Asian dust transported to the west coast of North America has an impact on the local air quality [Husar *et al*., 2001; McKendry *et al*., 2001]. Therefore, it is important to investigate the eastward transport efficiency of dust across the North Pacific.

The main objective of this study is to evaluate the eastward transport efficiency of dust across the North Pacific during 2007. Based on the observations from two satellite instruments – MODIS and CALIOP, I first estimated the flux of dust exported from the East Asia (over the northwest Pacific) and flux of dust imported to the west coast of the North America (over the northeast Pacific). Then, the transpacific transport efficiency of dust was derived by examining the difference between these two eastward fluxes.

Chapter *2* of the thesis provides a brief introduction of the methodology used in this study for computation of dust AOD, mass concentration, eastward flux, and eastward transport efficiency, with regard to each satellite data set. The MODIS and CALIOP results are compared and contrasted in Chapter *3*. At the end, Chapter *4* summarizes the main conclusions and proposes some future work.

Chapter 2: Methodology

2.1 MODIS Algorithm

The two parameters used for MODIS dust AOD (AOD_{du}) estimation were the columnar aerosol optical depth (AOD) and fine-mode fraction (f) retrievals from the MODIS/Terra Collection 5 level 3 daily aerosol products, gridded at 1° × 1° resolution. The computation was modified from Kaufman *et al*. (2005b)'s algorithm and followed the procedure below.

First, the daily dust AOD (AOD_{du}) was computed using Eqn.1 at individual 5° × 5° grids [Kaufman *et al*., 2005b].

$$AOD_{du} = \frac{AOD(f - f_a) - AOD_m(f_m - f_a)}{f_d - f_a} \qquad \text{(Eqn. 1)}$$

where AOD and f are the MODIS columnar AOD and aerosol find-mode fraction at 550 nm; AOD_m is the marine aerosol optical depth; f_d, f_m, and f_a are the fine-mode fraction corresponding to the dust, marine and anthropogenic aerosols, respectively. Instead of using the values proposed by Kaufman *et al*. (2005b), 0.37, 0.45, and 0.90 were applied to f_d, f_m, and f_a in order to better fit the MODIS Collection 5 data [Yu *et al*., 2009]. AOD_m was computed using Eqn. 2 [Kaufman *et al*., 2005b].

$$AOD_m = 0.007w + 0.02 \qquad \text{(Eqn. 2)}$$

where w is the surface wind speed in m/s, derived from the NCEP/DOE Reanalysis2 (http: //www.cdc.noaa.gov/) daily u-wind and v-wind products at 1000mb (at 2.5° × 2.5° resolution).

Next, the daily column dust mass concentration (M_{du}, g/m^2) was computed using Eqn.3 for each individual 5° × 5° grid [Kaufman *et al*., 2005b].

$$M_{du} = 2.7AOD_{du} \qquad \text{(Eqn. 3)}$$

The dust mass to dust optical depth ratio of 2.7 is selected based on collective results from studies using slightly different dust specific weight, dust particle effective radius, and light extinction efficiency [Haywood *et al*., 2003; Kaufman *et al*., 2005b; Maring *et al*., 2003].

Finally, the daily eastward dust flux (F_{du}, Tg) was obtained using Eqn. 4 [Kaufman *et al*., 2005b].

$$F_{du} = M_{du}uL \qquad \text{(Eqn. 4)}$$

where u is the eastward component of wind velocity in m/s, derived as the average of the NCEP/DOE Reanalysis2 (http: //www.cdc.noaa.gov/) daily u-winds from the pressure levels of 925, 850, 700, 600, 500, and 400 hPa (at 2.5° × 2.5° resolution); L is the longitudinal length of each box in m.

The daily F_{du} was then aggregated over the East Asia outflow region and the North America inflow region, respectively. The monthly eastward dust flux for each region was obtained by multiplying the mean daily F_{du} by the number of days of a specific month. The eastward transport efficiency of dust was computed as the inflow/outflow ratio.

2.2 CALIOP Algorithm

The two parameters used for CALIOP dust AOD (AOD_{du}) estimation were the aerosol columnar AOD (AOD) at 532 nm and volume depolarization ratio (VDR) retrievals from the CALIPSO Version 3 LIDAR level 2 5-km Aerosol Layer product, gridded at 5 km × 5 km resolution. The NASA CALIPSO Search and Subsetting Web Application tool (http://www-calipso.larc.nasa.gov/search/) was used to subset the CALIOP retrievals for the East Asia outflow and North America inflow regions. Computation of dust AOD was conducted using the following procedure.

First, using a threshold of 0.06, the CALIOP retrievals were separated into two groups – dust and non-dust. In the meantime, the number of aerosols in each group was counted. Dust was represented by retrievals with VDR equal or greater than 0.06 [Liu *et al*., 2008]. The percentage of dust was computed as the number of dust counts divided by the total aerosol counts. Then, AOD_{du} was computed as the observed daily aerosol columnar AOD multiplied by the above-derived percentage of dust. The estimation of the daily dust mass concentration (M_{du}), eastward dust flux (F_{du}), and eastward transport efficiency of dust followed the same procedure as described in Section 2.1 for MODIS data.

2.3 Studied Area

In order to evaluate the efficiency of trans-Pacific transport of dust, three boxes with a width of 10° in longitude were established on both sides of the North Pacific (Figure 2.1). Two boxes were located in the Northwest Pacific (NW Pacific): W1, centered at 140°E extending from 40°N to 60°N and W2, centered at 130°E extending from 20°N to 40°N. The third box was located in the Northeast Pacific (NE Pacific): E, centered at 130°W extending from 30°N to 60°N. The calculated eastward fluxes across Boxes W1 and W2 were integrated to represent the East Asia outflow of dust. The eastward dust flux across Box E was regarded as the North America inflow of dust.

Chapter 3: Trans-Pacific Transport of Dust – MODIS and CALIOP Assessment

In this chapter, the meridional variations of the annual eastward dust fluxes across the northwestern and northeastern Pacific during 2007 are first examined. Then, the seasonal variations of the integrated East Asia outflow and North America inflow of dust are assessed. The difference between the annual dust flux across the NW Pacific and that across the NE Pacific is used to evaluate the eastward transport efficiency of dust. The results from MODIS and CALIPSO are compared and contrasted. The satellite-based seasonal and annual fluxes of dust are further compared with the GFDL-GCTM model simulations. Possible reasons for the discrepancies between the results from different methods are discussed at the end of the thesis.

3.1 Meridional Variations of Dust Flux

The meridional variations of dust fluxes in the NW and NE Pacific were compared between the satellite estimates, as displayed in Figure 3.1. For the NW Pacific region, MODIS showed a maximum flux of 247 Tg $year^{-1}$ (~50% of the annual dust flux across the region) in the 30-40°N segment, followed by 95 and 92 Tg $year^{-1}$ in the 20-30°N and 40-50°N segments, respectively. A minimum dust flux of 60.9 Tg $year^{-1}$ was observed in the 50-60°N segment (Table 3.1). CALIOP observed the same geographic variation of the eastward flow of dust, but with magnitudes much lower than the MODIS observations (Table 3.1). The dust flux maximum between 30 and 40°N from CALIOP was 65.1 Tg $year^{-1}$ (~62% of the regional annual dust flux), about 4-fold lower than the MODIS estimate. The largest discrepancy existed in the northern segment, with the CALIOP

observation (5.18 Tg year^{-1}) being about 12-fold lower. However, the much higher MODIS estimate for this segment may be mainly caused by the lack of MODIS observation for this high latitude region in December and January of 2007, in which cases, the regional averages for the NW Pacific during that period were assigned to the missing values. Since high fluxes in the 30-40°N segment also contribute to the average, overestimate in dust flux in this northernmost segment is expected.

For the NE Pacific region, MODIS estimated the highest eastward flow of dust between 40 and 50°N, with a magnitude of 166 Tg year^{-1} (~52% of the regional annual dust flux) (Figure 3.1). The eastward dust flow decreased drastically towards the north and south. CALIOP also showed the same pattern, but revealing less drastic variation and having magnitudes of 12-17 times lower than MODIS.

The location of the dust flux peak in the East Asia outflow region in this study is in consistent with the model simulation by Uematsu *et al*. (2003). The patterns on both sides of the North Pacific indicate a poleward shift of dust flow during the transport from East Asia to the eastern North Pacific. This shift is characteristic for the trans-Pacific transport of dust and pollutants, which is governed by the atmospheric circulation in this region [Holzer *et al*., 2005].

3.2 Seasonal Variations of Dust Flux

On both sides of the North Pacific, MODIS showed the same seasonal pattern (Figure 3.2). The maximum dust flux occurred during springtime, with 257and 129 Tg for the

East Asia outflow and North America inflow regions, respectively. They were corresponding to 52 and 41% of the annual fluxes across these two regions. The minimum dust flux was observed in summer, with 48.2 and 24.0 Tg for the NW and NE Pacific, corresponding to about 10% of the annual flux. Dust flux in winter was lower than that in spring, and the fall dust flux was intermediate between those in summer and winter (Table 3.2). The flux peak observed by MODIS during springtime is in accordance with general timing of dust season in East Asia [Qian *et al*., 2002]. The relatively high wintertime dust fluxes may be resulted from having stronger eastward winds during this particular year for transport compared with other seasons. The minimum dust flux in summer may be a synergistic effect due to low dust frequency and high precipitation rates in East Asia and low winds in the North Pacific during this season. In general, the seasonal variations of the eastward dust flux observed by MODIS agree with the seasonality of the meteorological conditions in this region, which support efficient export of aerosols from source regions during spring and winter and intermediate transport in the fall [Holzer *et al*., 2005].

Again, CALIOP revealed the same seasonal pattern but significantly lower in the magnitude of dust flux (Figure 3.2). As shown in Figure 3.2, MODIS seasonal fluxes were 4 to 6 times higher than those of CALIOP in the East Asia outflow region, 13 to 22 times higher in the North America inflow region. The MODIS-CALIOP discrepancy was greatest in summer, which was a low-dust season. Although greatly different in magnitude, the seasonal dust contributions to the annual flux in percentage agreed well between these two satellite approaches (Table 3.2).

The seasonal variations of eastward dust flow were also compared with the GCTM simulation. As seen in Figure 3.2, in general GCTM simulated even lower eastward dust fluxes, compared with the satellite approaches. In summer, the GCTM simulation was comparable with the CALIOP observation. Contrastingly, in other seasons, GCTM simulated eastward dust fluxes of 2.5 to 9 times lower than CALIOP in the NW Pacific, and 3 to 24 times lower in the NE Pacific. Although still showing that the highest eastward dust flux occurred in spring (~60% contribution to the annual dust flux), GCTM simulated a different pattern for the other seasons – lowest fluxes in winter, and higher fluxes summer than those in fall. As a result, the dust contribution by each season to the annual flux differed greatly between the model simulation and the satellite observations.

3.3 Eastward Transport Efficiency of Dust

In the work by Kaufman *et al*. (2005), the dust deposition into the tropical Atlantic was estimated by looking at the difference in westward dust fluxes across the 15°W and 75°W longitudinal lines. This approach, however, is not suitable for the North Pacific region. This is mainly due to the different meteorological conditions overlying these two oceanic regions. The winds are fairly steady for the tropical Atlantic, with the easterly trade winds prevailing throughout the year. In contrast, wind conditions are much more variable and complicated in the North Pacific [Holzer *et al*., 2005]. Winds changes directions throughout the year. In addition, dust events in East Asia are usually associated with cyclone cold fronts during late winter and early spring [Qian *et al*., 2002]. Other than the eastward transport of dust, a north-south component also exists [Holzer *et al*., 2005]. Therefore, by simply looking at the difference in dust flux on both sides of the North

Pacific, we cannot obtain an accurate estimate for the dust deposition into this oceanic area. Nonetheless, the discrepancy in eastward dust flux on both sides of the North Pacific can serve as a good proxy to evaluate the eastward transport efficiency of Asian dust across this oceanic region.

As shown in Table 3.3, MODIS estimated eastward transport efficiency of 50 to 77% during winter, spring, and summer. The transport efficiency during the same periods turned out to be much lower from CALIOP, ranging from 15 to 33%. Both satellite approaches suggested higher eastward transport efficiency in winter than in other seasons. In fall, a net westward flux was indicated by MODIS, which was absent in the CALIOP estimation. Compared with the satellite approaches, GCTM suggested a relatively stable transport efficiency throughout the year, ranging from 12 to 16%.

On an annual basis, the MODIS estimation of the dust outflow and inflow was 494 and 318 Tg, respectively, corresponding to an annual transport efficiency of 64%. In comparison, CALIOP estimated the dust outflow and inflow of 104 and 22.6 Tg, leading to an annual mean transport efficiency of 22%. GCTM simulated an annual eastward dust transport efficiency of 13%, which was corresponding to the annual outflow and inflow of 38.6 and 4.98 Tg dust, respectively (Figure 3.3).

3.4 Remarks on the Discrepancies in MODIS and CALIOP estimates

The estimation of the East Asia outflow and North America inflow of dust differed significantly in magnitude between the MODIS and CALIOP, as well as between the satellite estimation and GCTM simulation. In this study, the estimates of dust flux by MODIS were apparently greater than those by the other two approaches.

As we know, the magnitude of the estimated dust flux is very sensitive to the applied wind field. It is also affected by the estimation of dust mass concentration in the air column. Since the difference in wind fields applied in the two satellite approaches was minor (Tables A.1 and A.2), the observed great discrepancy in dust flux should be due to the differences in dust AOD and dust mass concentration estimation by MODIS and CALIOP. Based on the AOD and AOD_{du} data from Tables A.1 and A.2, Figure 3.4 was plotted to display the time-series of the observed total column AOD and the estimated dust AOD for 2007 in the East Asia outflow and North America inflow regions by MODIS and CALIOP. I further calculated the annual averages of the observed column AOD and the estimated AOD_{du} by MODIS and CALIOP. Then, according to these annual averages, I examined i) the dust to total AOD ratio in the outflow region – $(AOD_{du}/AOD)_{out}$, ii) the dust to total AOD ratio in the inflow region – $(AOD_{du}/AOD)_{in}$, and iii) the ratio of dust AOD in the inflow region to that in the outflow region – $AOD_{du,in}/AOD_{du,out}$ from MODIS and CALIOP. The results are summarized in Table 3.4. It can be seen that in 2007:

1) MODIS observed much higher columnar AOD than CALIOP on both sides of the North Pacific (Figure 3.4 and Table 3.4). Consequently, the estimation of dust AOD

started with a much higher columnar AOD in the MODIS approach than in the CALIOP method.

2) On both sides of the North Pacific, the dust to total AOD ratio was higher in the MODIS method than in the CALIOP approach (Table 3.4).

3) The MODIS inflow/outflow ratio for dust AOD was much higher than the CALIOP ratio (Table 3.4), in accordance with higher estimation of transport efficiency by MODIS.

All three findings could be explained by a scenario in which CALIOP either misses the major dust event, or misidentifies dust as clouds. The former could be due to the long repeating cycle of CALIOP (~16 days). And as mentioned in Chapter 1, the misidentification issue was also noticed by previous researchers [Liu *et al*., 2008; Yu *et al*., 2010].

In spite of the likelihood of CALIOP underestimation, the dust fluxes estimated by CALIOP should be closer to reality than by MODIS, based on the examination of the magnitude of estimated fluxes, and the comparison between the satellite-estimated dust mass concentration with *in situ* measurements from nearby regions (personal communication with Dr. S. Fan). In fact, overestimation of dust AOD by MODIS can also explain the above findings. There are several possible reasons for MODIS overestimation. One is the lack of a lower boundary for f values in dust AOD computation in this study. It has been realized that inclusion of low f values in computation could result in an increase in dust AOD estimate. Another reason may be due to using a constant fine-mode fraction for marine aerosols (f_m) in dust AOD estimation. Yu *et al*. (2009) applied

seasonally and geographically variable f_m values to study the transport of anthropogenic aerosols across the North Pacific. They argued that by using a constant f_m, the anthropogenic AOD could be overestimated by about 20% over global ocean. Similarly, an overestimate of dust AOD may also occur due to the usage of a constant f_m. Finally, as mentioned in Chapter 1, it has been noticed that MODIS easily suffers from cloud contamination and tends to bias AOD high in the NW Pacific [Remer et al., 2005; Yu *et al*., 2010].

The discrepancy in AOD observations may be resulted from instrumental differences in MODIS and CALIOP, with the former being a passive imager measuring the radiance at 550 nm and the latter an active lidar measuring the backscattering of light at 532 nm. However, since CALIPSO validation is still underway, how much the difference could be has not determined completely.

3.5 Remarks on the Discrepancies in MODIS/CALIOP and GCTM estimation

As GCTM is validated by comparing the model simulated dust column concentrations with the *in situ* measured dust concentrations, not with the real dust flux measurements, it is possible to see discrepancies in dust flux estimation between the remote-sensing estimation and model simulations. In the North Pacific, observations from limited stations are available to compare with the model outputs, and thus, dust flux estimates by satellites should be valuable to complement the model simulated dust fluxes to this oceanic region and to the improvement of model parameterization.

3.6 Remarks on the CALIOP method

For the CALIOP approach used in this study, I have realized that it is better to use the 'Feature_Optical_Depth_532' parameter to derive the dust AOD than using 'Column_Optical_Depth_Aerosols_532'. The former is a layer descriptor and sampled simultaneously with the layer property VDR. The latter, although also a CALIPSO level 2 aerosol product, describes the column property, provided in a grid different from that for the VDR records. It is not straightforward to directly combine 'Column_Optical_Depth_Aerosols_532' with VDR retrievals. Nonetheless, re-computing the dust AOD and flux by using 'Feature_Optical_Depth_532' will not significantly reduce the difference between the MODIS and CALIOP estimates. The reason is that dust AOD derived from 'Feature_Optical_Depth_532' will not exceed the observed total column AOD, which is corresponding to 'Column_Optical_Depth_Aerosols_532' retrievals. Based on the total columnar AOD comparison shown in Figure 3.4, the dust flux derived from 'Feature_Optical_Depth_532' is expected to be still much lower than the MODIS estimation in this study. Other than the choice of parameter, another important factor not considered by this study is the sea-salt influence. Also being non-spherical, sea-salt can exert similar influence on CALIOP AOD retrievals as dust particles. By ignoring the sea-salt effect, this study may have overestimated the dust AOD and flux. Another problem in this CALIOP study is the lack of data screening. AOD retrievals from CALIOP can be significantly contaminated by low-altitude clouds. Large uncertainties can also be generated when CALIOP retrieves AOD under very noisy conditions. Without screening out the problematic AOD retrievals, the estimated dust AOD and flux might contain great uncertainties.

In this study, a VDR threshold of 0.06 was used to differentiate the dust from other aerosols [Liu *et al*., 2008; Yu *et al*. 2010]. Using this threshold, some pollutant/smoke mixed with dust would also be identified as dust, thus resulting in an overestimate in dust flux. Based on the current CALIPSO product, it is still challenging to separate AOD solely contributed by dust in the column. However, the 0.06 dust threshold may allow us to have a good estimation on the upper limit of dust fluxes, which is valuable for budgeting the global aerosol radiative forcing and validating dust models.

Chapter 4: Major Conclusions and Future Work

The major conclusions drawn from this study include:

1) Both satellite approaches observed distinct meridional variations of the eastward dust flux. In the East Asia outflow region, maximum dust flux occurred between 30 and 40°N. The dust flow shifted poleward after the trans-Pacific transport and peaked between 40 and 50°N in the North America inflow region.

2) Both satellite approaches revealed the same seasonal pattern of dust transport – maximum in spring, minimum in summer, relatively high in winter, and intermediate in fall between that in summer and winter. Despite large discrepancies in magnitude, the percentages of the seasonal contributions to the annual dust fluxes agreed well between the MODIS and CALIOP estimates. This satellite-observed seasonal pattern was different from that simulated by GCTM. Though also having the spring maximum, GCTM showed comparable dust fluxes in winter and fall which were both significantly lower than that in summer.

3) The annual efficiency of the eastward dust transport was 64% as estimated by MODIS, and 22% by CALIOP. Both approaches indicated seasonal variations in transport efficiencies with high efficiency observed in winter. In contrast, GCTM simulated relatively constant transport efficiencies throughout the year, averaged 13% for 2007.

4) Overall, MODIS estimated greater dust fluxes than CALIOP, by about 5-fold for the NW Pacific and 14-fold for the NE Pacific. GCTM simulated even lower dust fluxes than CALIOP.

Future work can be done to improve the CALIOP estimation:

1) Data screening is better to be performed using 'Feature_Classification_Flags' (to exclude retrievals associated with the presence of low-altitude clouds and sea-salt) and 'ExtinctionQC_532' (to screen out retrievals with large uncertainties). The first criterion turns out to be necessary for the CALIOP AOD retrievals, while the second criterion might be a secondary consideration. The data screening process will help reduce the uncertainties in CALIOP estimation.

2) CALIOP dust AOD should be derived using the following procedure:

i) Use 'Feature_Classification_Flags' and 'Layer_Top_Altitude' to screen out AOD retrievals associated with the existence of low-altitude cloud and sea-salt.

ii) Use a VDR threshold of 0.06 to obtain all dust records in the atmospheric column and compute the average 'Feature_Optical_Depth_532'. Meanwhile, count the number of dust records and the total number of aerosol detected to get the percentage of dust count in the column.

iii) Obtain the dust AOD by multiplying the average 'Feature_Optical_Depth_532' with the number percentage of the dust.

Bibliography

Carlson, T. N. (1979), Atmospheric turbidity in Saharan dust outbreaks as determined by analysis of satellite brightness data, *Mon. Weather Rev*., 107, 322–335.

Chin, M., P. Ginoux, R. Lucchesi, B. Huebert, R. Weber, T. Anderson, S. Masonis, B. Blomquist, A. Bandy, and D. Thornton (2003), A global aerosol model forecast for the ACE-Asia field experiment, *J. Geophys. Res*., 108(D23), 8654, doi:10.1029/2003JD003642.

Denman, K. L., et al. (2007), Couplings between changes in the climate system and biogeochemistry, in *Climate Change 2007: The Physical Science Basis. Contribution of Working Group I to the Fourth Assessment Report of the Intergovernmental Panel on Climate Change*, edited by S. Solomon et al., pp. 488-587, Cambridge Univ. Press, Cambridge, U. K.

Duce, R. A., C. K. Unni, B. J. Ray, J. M. Prospero, and J. T. Merrill (1980), Long-range atmospheric transport of soil dust from Asia to the tropical North Pacific: Temporal variability, *Science*, 209, 1522-1524.

Duce et al. (1991), The atmospheric input of trace species to the world ocean, *Global Biogeochem. Cycles*, 5(3), 193-259.

Duce, R. A. and N. W. Tindale (1991), Atmospheric transport of iron and its deposition in the ocean, *Limnol. Oceanogr.*, 36, 1715–1726.

Forster, P., et al. (2007), Changes in atmospheric constituents and in radiative forcing, in *Climate Change 2007: The Physical Science Basis. Contribution of Working Group I to the Fourth Assessment Report of the Intergovernmental Panel on Climate Change*, edited by S. Solomon et al., pp. 129-234, Cambridge Univ. Press, Cambridge, U. K.

Gao, Y., R. Arimoto, R.A. Duce, X.Y. Zhang, G.Y. Zhang, Z.S. An, L.Q. Chen, M.Y. Zhou, and D.Y. Gu (1997), Temporal and spatial distributions of dust and its deposition to the China Sea, *TelluB*, 49, 172-189.

Gao, Y., Y.J. Kaufman, D. Tanré, D. Kolber, and P.G.Falkowski (2001), Seasonal distribution of Aeolian iron fluxes to the global ocean, *Geophys. Res. Lett*., 28(1), 29-32.

Gao, Y., S.-M. Fan, and J. L. Sarmiento (2003), Aeolian iron input to the ocean through precipitation scavenging: A modeling perspective and its implication for natural iron fertilization in the ocean, *J. Geophys. Res*., 108(D7), 4221, doi:10.1029/2002JD002420.

Gassó, S. and A. F. Stein (2007), Does dust from Patagonia reach the sub-Antarctic Atlantic Ocean?, *Geophys. Res. Lett*., 34, L01801, doi:10.1029/2006GL027693.

Gautam, R., Z. Liu, R. P. Singh, and N. C.Hsu (2009), Two contrasting dust-dominant periods over India observed from MODIS and CALIPSO data, *Geophys. Res. Lett*., 36, L06813, doi:10.1029/2008GL036967.

Ginoux, P. and O. Torres (2003), Empirical TOMS index for dust aerosol: Applications to model validation and source characterization, J. Geophys. Res., 108(D17), 4534, doi:10.1029/2003JD003470.

Haywood, J., and O. Boucher (2000), Estimates of the direct and indirect radiative forcing due to tropospheric aerosols: A review, *Rev. Geophys*., 38(4), 513-543, doi:10.1029/1999RG000078.

Herman, J. R., *et al*. (1997), Global distribution of UV-absorbing aerosol from Nimbus-7/TOMS data, J. Geophys. Res., 102, 16,911 – 16,922.

Holzer, M., T. M. Hall, and R. B. Stull (2005), Seasonality and weather-driven variability of transpacific transport, J. Geophys. Res., 110, D23103, doi:10.1029/2005JD006261.

Huang, J., P. Minnis, B. Chen, Z. Huang, Z. Liu, Q. Zhao, Y. Yi, and J. K. Ayers (2008), Long-range transport and vertical structure of Asian dust from CALIPSO and surface measurements during PACDEX, *J. Geophys. Res*., 113, D23212, doi:10.1029/2008JD010620.

Huang, J., C. Zhang, and J. M. Prospero (2009), Aerosol-Induced Large-Scale Variability in Precipitation over the Tropical Atlantic, *J. Clim.*, 22(19), 4970-4988, doi: 10.1175/2009JCLI2531.1.

Husar, R. B., Tratt, D. M., Schichtel, B. A., Falke, S. R., Li, F., Jaffe, D., Gassó, S., Gill, T., Lanlainen, N. S., Lu, F., Reheis, M. C., Chun, Y., Westphal, D., Holben, B. N., Gueymard, C., McKendry, I., Kuring, N., Feldman, G. C., McClain, C., Frouin, R. J., Merrill, J., DuBois, D., Vignola, F., Murayama, T., Nickovic, S., Wilson,W. E., Sassen K., Sugimoto, N., and Malm,W. C. (2001), Asian dust events of April 1998, *J. Geophys. Res.*, 106D, 18,317-18,330.

Hsu, S.-C., S. C. Liu, R. Arimoto, T.-H. Liu, Y.-T. Huang, F. Tsai, F.-J. Lin, and S.-J. Kao (2009), Dust deposition to the East China Sea and its biogeochemical implications, *J. Geophys. Res*., 114, D15304, doi:10.1029/2008JD011223.

Jaffe, D. A., T. Anderson, D. Covert, R. Kotchenruther, B. Trost, J. Danielson, W. Simpson, T. Berntsen, S. Karlsdottir, D. Blake, J. Harris, G. Carmichael, and I. Uno (1999), Transport of Asian Air Pollution to North America. *Geophys.Res.Letts*. 26, 711-714.

Jickells, T. D. and L. J. Spokes (2001), Atmospheric iron inputs to the ocean, in *Biogeochemistry of Iron in Seawater*, edited by D. Turner and K. A. Hunter, pp. 85–121, John Wiley, New York.

Jickells, T.D., et al. (2005), Global Iron Connections Between Desert Dust, Ocean Biogeochemistry, and Climate, *Science*, 308, 67, doi: 10.1126/science.1105959.

Kaufman, Y. J., I. Koren, L. A. Remer, D. Rosenfeld, and Y. Rudich (2005a), The effect of smoke, dust and pollution aerosol on shallow cloud development over the Atlantic Ocean, *Proc. Natl. Acad. Sci. U. S. A.*, 102,11,207–11,212.

Kaufman, Y. J., I. Koren, L. A. Remer, D. Tanré, P. Ginoux, and S. Fan (2005b), Dust transport and deposition observed from the Terra-Moderate Resolution Imaging Spectroradiometer (MODIS) spacecraft over the Atlantic Ocean, *J. Geophys. Res*., 110, D10S12, doi:10.1029/2003JD004436.

Kwon, S. A.,Y. Iwasaka, T. Shibata, and T. Sakai (1997),Vertical distribution of atmospheric particles and water vapor densities in the free troposphere: Lidar

measurement in spring and summer in Nagoya, Japan, *Atmos. Environ.*, 31, 1459–1465, doi:10.1016/S1352-2310(96)00310-X.

Li, R. and Q.-L. Min (2010), Impacts of mineral dust on the vertical structure of precipitation, J. Geophys. Res., 115, D09203, doi:10.1029/2009JD011925.

Liu, D., Z. Wang, Z. Liu, D. Winker, and C. Trepte (2008), A height resolved global view of dust aerosols from the first year CALIPSO lidar measurements, J. Geophys. Res., 113, D16214, doi:10.1029/2007JD009776.

Maring, H., D. L. Savoie, M. A. Izaguirre, L. Custals, and J. S. Reid (2003), Mineral dust aerosol size distribution change during atmospheric transport, *J. Geophys. Res*., 108(D19), 8592, doi:10.1029/2002JD002536.

Martins, J.V., D. Tanré, L. Remer, Y. Kaufman, S. Mattoo, and R. Levy (2002), MODIS cloud screening for remote sensing of aerosols over oceans using spatial variability, *Geophys. Res. Lett*., 29(12), doi:10.1029/2001GL013252.

Masuzawa, T., S. Noriki, T. Kurosaki, S. Tsunogai, and M. Koyama (1989), Compositional change of settling particles with water depth in Japan Sea, *Mar. Chem*., 27 (1), 61–78, doi:10.1016/0304-4203(89)90028-5.

McKendry, I. G., J. P. Hacker, R. Stull, S. Sakiyama, D. Mignacca, and K. Reid (2001), Long-range transport of Asian dust to the Lower Fraser Valley, British Columbia, Canada, *J. Geophys. Res.*, *106*(D16), 18, 361–18, 370.

Prospero, J. M., and T. N. Carlson (1972), Vertical and areal distribution of Saharan dust over the western equatorial North Atlantic ocean, J. Geophys. Res., 77, 5255– 5265.

Prospero, J. M., and R. T. Nees (1977), Dust concentration in the atmosphere of the equatorial North Atlantic Possible relationship to Sahelian drought, Science, 196, 1196–1198.

Prospero, J. M., P. Ginoux, O. Torres, S. E. Nicholson, and T. E. Gill (2002), Environmental characterization of global sources of atmospheric soil dust identified with the NIMBUS 7 Total Ozone Mapping Spectrometer (TOMS) absorbing aerosol product, *Rev. Geophys*., 40(1), 1002, doi:10.1029/2000RG000095.

Qian, W., L. Quan, and S. Shi (2002), Variations of the Dust Storm in China and its Climatic Control, J. Climate, 15, 1216-1229.

Remer, L. A., et al. (2005), The MODIS aerosol algorithm, products, and validation, *J. Atmos. Sci*., 62, 947-973, doi:10.1175/JAS3385.1.

Rosenfeld, D., Y. Rudich, and R. Lahav (2001), Desert dust suppressing precipitation: A possible desertification feedback loop, Proc. Natl. Acad. Sci. U. S. A., 98, 5975–5980.

Sun, J., M. Zhang, and T. Liu (2001), Spatial and temporal characteristics of dust storms in China and its surrounding regions, 1960–1999: Relations to source area and climate, *J. Geophys. Res.*, 106, 10,325–10,333, doi:10.1029/2000JD900665.

Taylor, S. R. and S. M. McLennan (1985), The Continental Crust: Its Composition and Evolution, pp. 312 , Blackwell Scientific, Oxford.

Uematsu, M., R.A. Duce, J.M. Prospero, L. Chen, J.T. Merrill, and R.L. McDonald (1983), Transport of mineral aerosol from Asia over the North Pacific Ocean, *J. Geophys.Res., 88*(C9), 5343-5352.

Uematsu, M., R.A. Duce, and J.M. Prospero (1985), Deposition of atmospheric mineral particles in the North Pacific Ocean, *J. Atmos. Chern*., 3, 123-138.

Uematsu, M., Z. Wang, and I. Uno (2003), Atmospheric input of mineral dust to the western North Pacific region based on direct measurements and a regional chemical transport model, Geophys. Res. Lett. , 30 (6), 1342, doi:10.1029/2002GL016645.

Wang, X., Z. Dong, J. Zhang, and. Liu (2004), Modern dust storms in China: An overview, *J. Arid Environ*., 58, 559–574, doi:10.1016/j.jaridenv.2003.11.009.

Winker, D. M., J. R. Pelon, and M. P. McCormick (2003), The CALIPSO mission: Spaceborne lidar for observation of aerosols and clouds, *Proc. SPIE*, 4893, 1–11.

Winker, David M., Mark A. Vaughan, Ali Omar, Yongxiang Hu, Kathleen A. Powell,

Yu, H., M. Chin, L. A. Remer, R. G. Kleidman, N. Bellouin, H. Bian, and T. Diehl (2009), Variability of marine aerosol fine-mode fraction and estimates of anthropogenic aerosol component over cloud-free oceans from the Moderate Resolution Imaging Spectroradiometer (MODIS), *J. Geophys. Res*., 114, D10206, doi:10.1029/2008JD010648.

Yu, H., M. Chin, D. M. Winker, A. H. Omar, Z. Liu, C. Kittaka, and T. Diehl (2010), Global view of aerosol vertical distributions from CALIPSO lidar measurements and GOCART simulations: Regional and seasonal variations, *J. Geophys. Res*., 115, D00H30, doi:10.1029/2009JD013364.

Zhang, H., G. M. McFarquhar, W. R. Cotton, and Y. Deng (2009), Direct and indirect impacts of Saharan dust acting as cloud condensation nuclei on tropical cyclone eyewall development, *Geophys. Res. Lett*., 36, L06802, doi:10.1029/2009GL037276

Table 3.1 Comparisons of the meridional variations of MODIS and CALIOP observations of columnar AOD and estimates of dust AOD (AOD_{du}), mass concentration (M_{du}), and eastward flux (F_{du}) in the East Asia outflow (a) and North America inflow (b) regions.

(a)

Lat	MODIS				CALIOP				MOD/CAL
	AOD	AOD_{du}	M_{du} (g/m^2)	F_{du} (Tg/year)	AOD	AOD_{du}	M_{du} (g/m^2)	F_{du} (Tg/year)	
60-50N	0.247	0.153	0.412	60.9	0.0794	0.0173	0.0467	5.18	12
50-40N	0.284	0.126	0.341	92	0.099	0.0222	0.0601	18.7	4.9
40-30N	0.406	0.195	0.527	247	0.153	0.0479	0.129	65.1	3.8
30-20N	0.257	0.111	0.299	95	0.0894	0.0125	0.0337	15.3	6.2

(b)

Lat	MODIS				CALIOP				MOD/CAL
	AOD	AOD_{du}	M_{du} (g/m^2)	F_{du} (Tg/year)	AOD	AOD_{du}	M_{du} (g/m^2)	F_{du} (Tg/year)	
60-50N	0.189	0.132	0.357	84.3	0.0550	0.0115	0.0312	7.27	12
50-40N	0.227	0.137	0.371	166	0.0621	0.00893	0.0241	10.0	17
40-30N	0.158	0.0803	0.217	67.8	0.0463	0.00688	0.0186	5.28	13

Table 3.2 Comparisons of the seasonal variations of eastward fluxes of dust estimated by MODIS (a) and CALIOP (b) and GCTM (c) in the East Asia outflow and North America inflow regions.

(a)

Season	East Asia Outflow (Tg)	seasonal/annual, %	North America Inflow (Tg)	seasonal/annual, %
winter	126	26	97	31
spring	257	52	129	40
summer	48.2	10	24.0	7.5
fall	62.2	13	68.4	22

(b)

Season	East Asia Outflow (Tg)	seasonal/annual, %	North America Inflow (Tg)	seasonal/annual, %
winter	23.5	23	7.78	34
spring	58.8	56	9.4	41
summer	7.61	7.3	1.11	4.9
fall	14.3	14	4.35	19

(c)

Season	East Asia Outflow (Tg)	seasonal/annual, %	North America Inflow (Tg)	seasonal/annual, %
winter	2.60	6.7	0.329	6.6
spring	23.7	62	2.87	58
summer	8.46	22	1.35	27
fall	3.76	10	0.43	8.7

Table 3.3 Comparisons of the eastward transport efficiencies of dust across the North Pacific estimated by MODIS (a), CALIOP (b), and GCTM (c).

(a)

	East Asia Outflow (Tg)	North America Inflow (Tg)	Inflow/Outflow (%)
winter	126	97	77
spring	257	129	50
summer	48.2	24.0	50
fall	62.2	68.4	110
Annual Total	494	318	64

(b)

	East Asia Outflow (Tg)	North America Inflow (Tg)	Inflow/Outflow (%)
winter	23.5	7.78	33
spring	58.8	9.4	16
summer	7.61	1.11	15
fall	14.3	4.35	30
Annual Total	104	22.6	22

(c)

	East Asia Outflow (Tg)	North America Inflow (Tg)	Inflow/Outflow (%)
winter	2.60	0.329	13
spring	23.7	2.87	12
summer	8.46	1.35	16
fall	3.76	0.433	12
Annual Total	38.6	4.98	13

Table 3.4 Comparisons of the annual averages of column AOD in the outflow (AOD_{out}) and inflow (AOD_{in}) regions, the annual averages of dust AOD in the outflow ($AOD_{du,out}$) and inflow ($AOD_{du,in}$) regions, the annually averaged dust to total AOD ratio in the outflow region ($(AOD_{du}/AOD)_{out}$), the annually averaged dust to total AOD ratio in the inflow region ($(AOD_{du}/AOD)_{in}$), and the ratio of the annually averaged dust AOD in the inflow region to that in the outflow region ($AOD_{du,in}/AOD_{du,out}$) from MODIS and CALIOP in 2007.

	MODIS	**CALIOP**
AOD_{out}	0.299	0.105
AOD_{in}	0.190	0.0544
$AOD_{du,out}$	0.144	0.0250
$AOD_{du,in}$	0.116	0.0091
$(AOD_{du}/AOD)_{out}$	0.48	0.24
$(AOD_{du}/AOD)_{in}$	0.61	0.17
$AOD_{du,in}/AOD_{du,out}$	0.81	0.37

List of Figures:

Figure 2.1

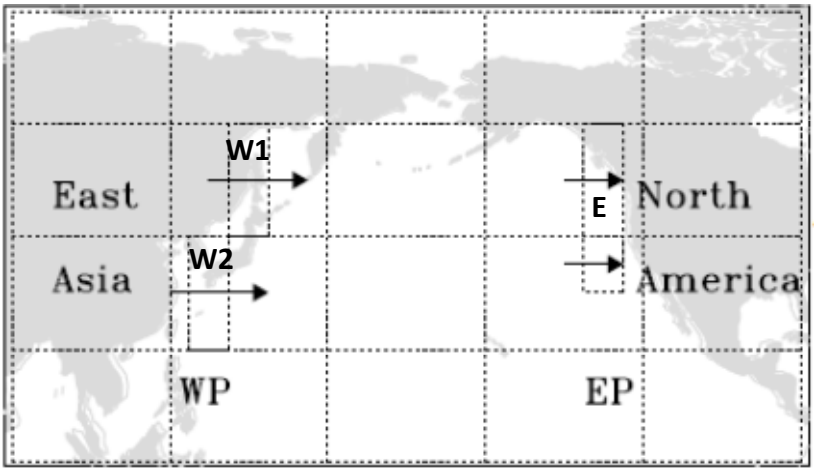

Figure 3.1

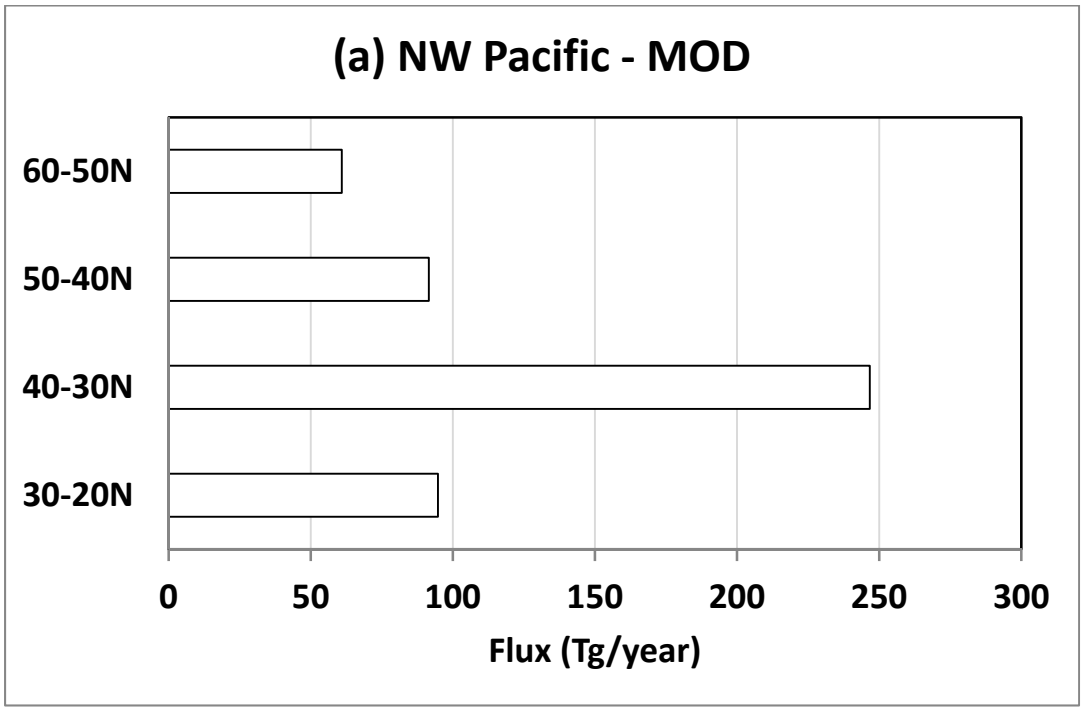
(a) NW Pacific - MOD
60-50N
50-40N
40-30N
30-20N
0
50
100
150
200
250
300
Flux (Tg/year)

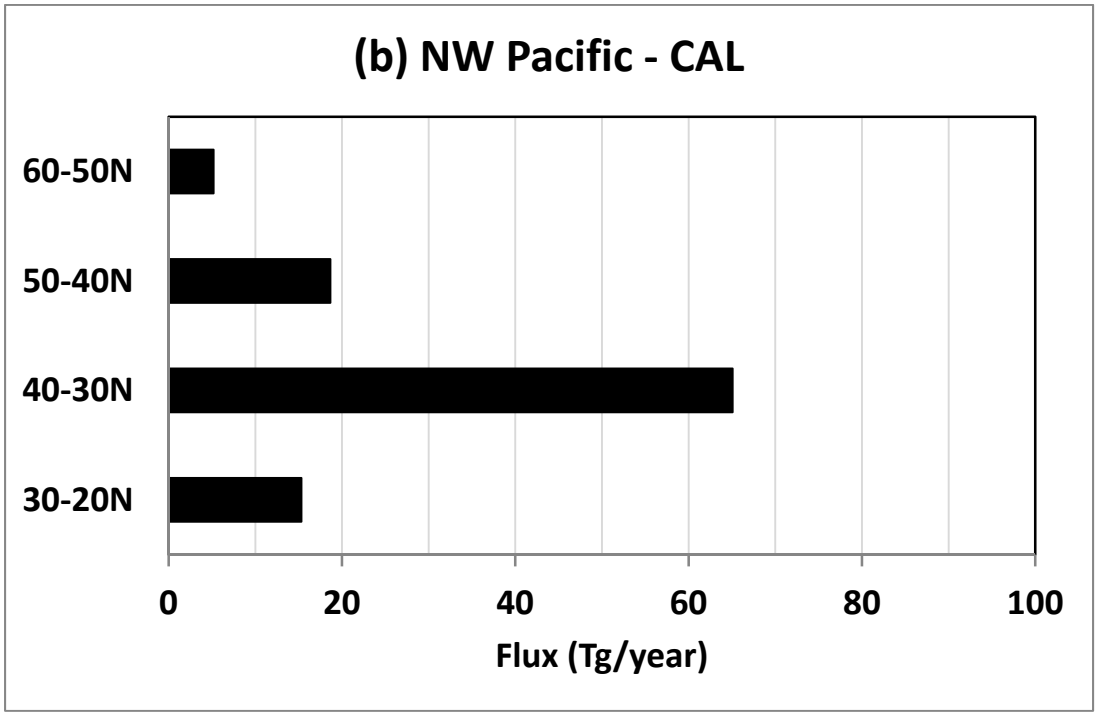
(b) NW Pacific - CAL
60-50N
50-40N
40-30N
30-20N
0
20
40
60
80
100
Flux (Tg/year)

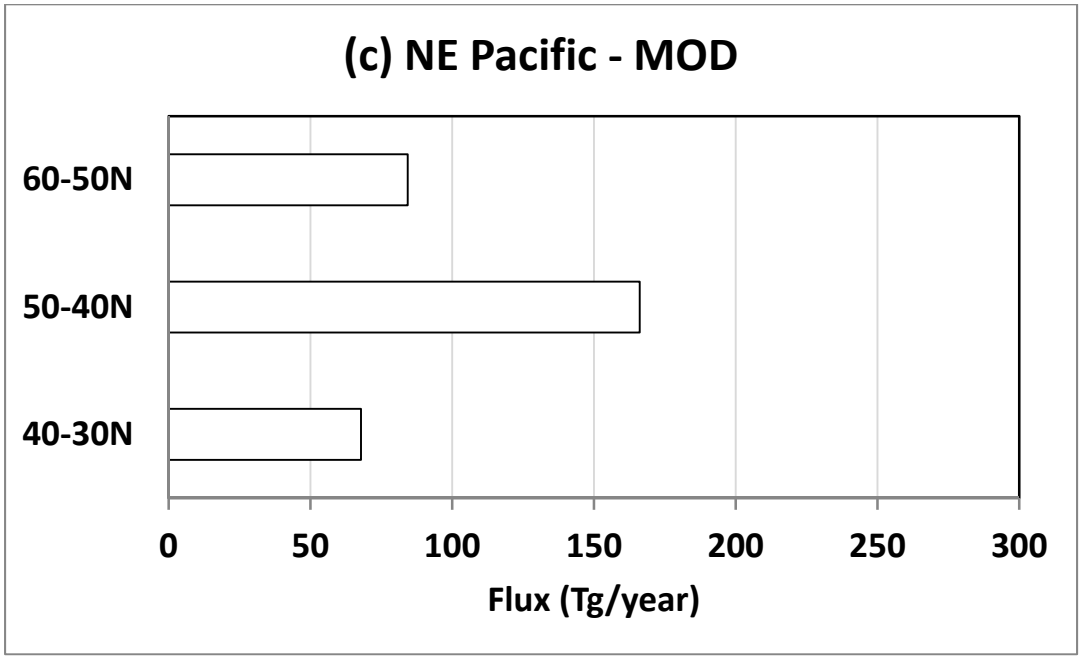
(c) NE Pacific - MOD
60-50N
50-40N
40-30N
0
50
100
150
200
250
300
Flux (Tg/year)

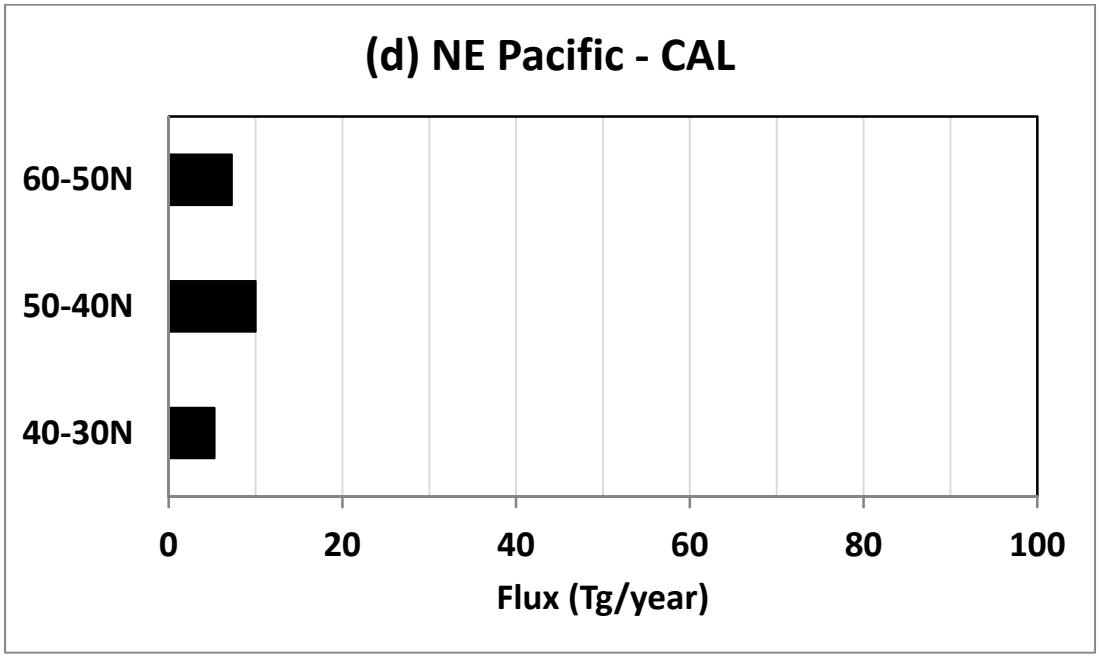
(d) NE Pacific - CAL
60-50N
50-40N
40-30N
0
20
40
60
80
100
Flux (Tg/year)

Figure 3.2

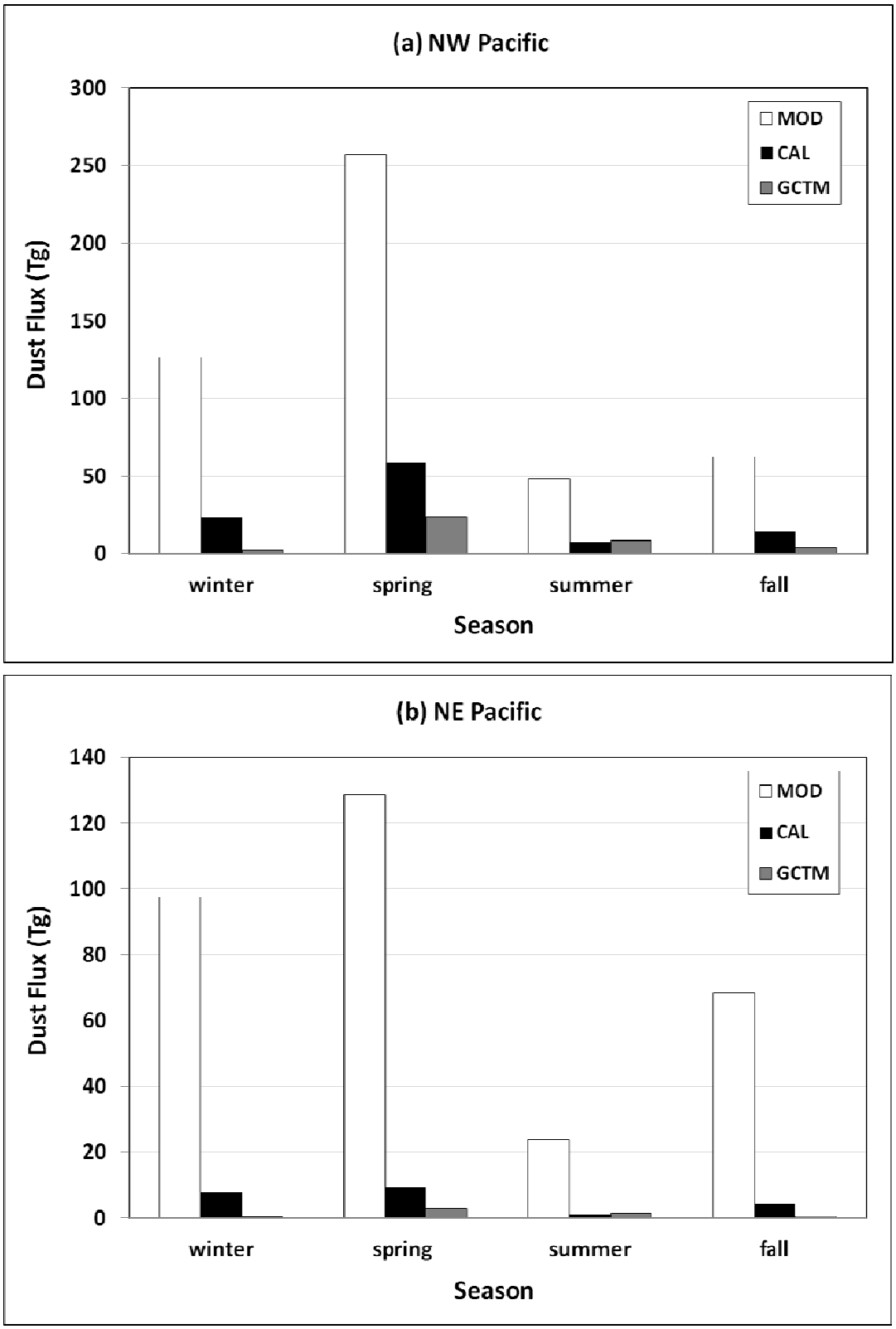
(a) NW Pacific
300
250
200
150
100
50
0
Dust Flux (Tg)
MOD
CAL
GCTM
winter
spring
summer
fall
Season
(b) NE Pacific
140
120
100
80
60
40
20
0
Dust Flux (Tg)
MOD
CAL
GCTM
winter
spring
summer
fall
Season

Figure 3.3

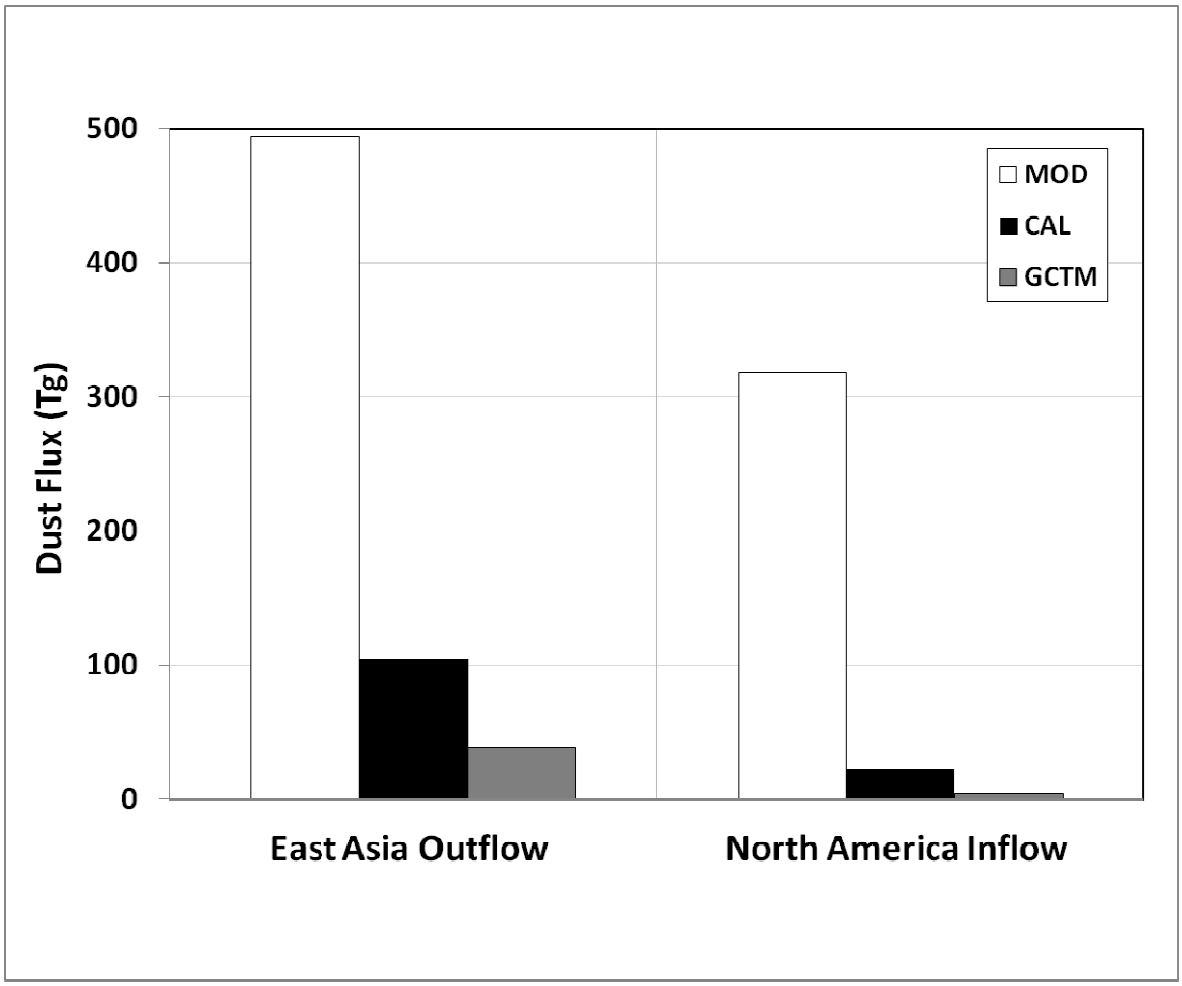
500
400
300
200
100
0
Dust Flux (Tg)
MOD
CAL
GCTM
East Asia Outflow
North America Inflow

Figure 3.4

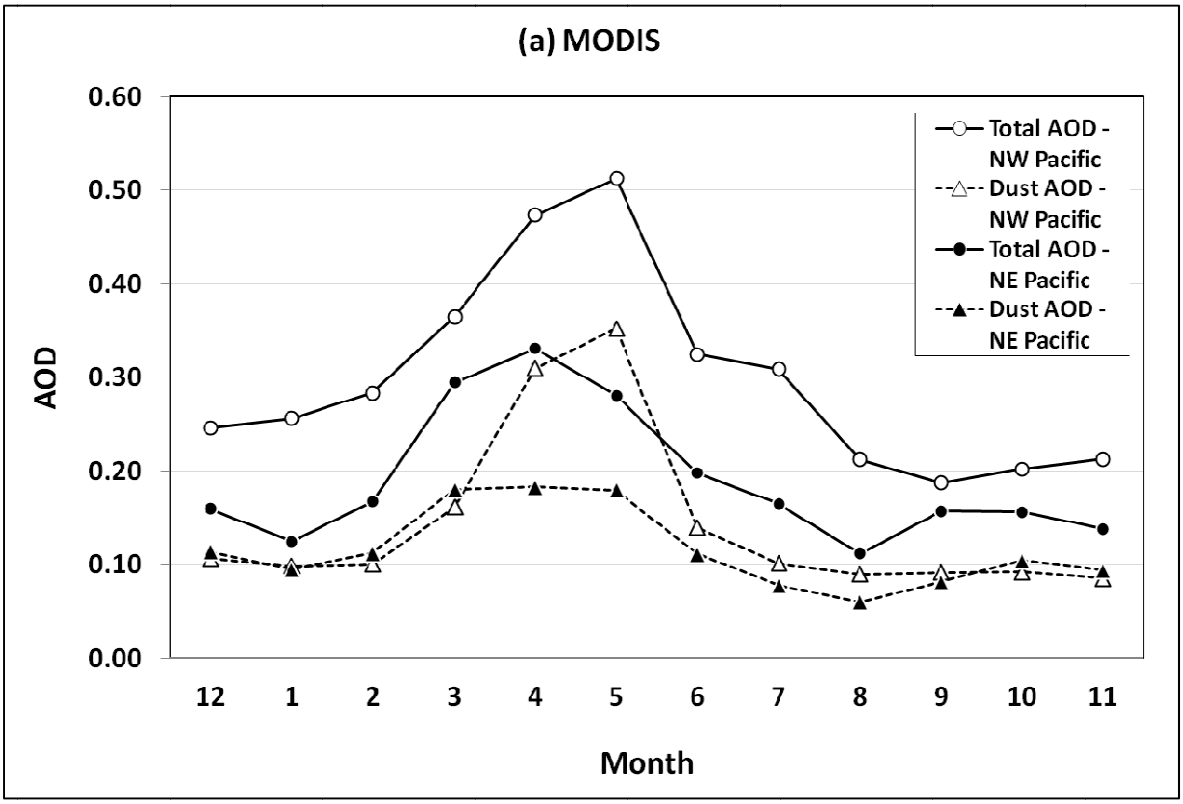
(a) MODIS
AOD
0.60
0.50
0.40
0.30
0.20
0.10
0.00
12
1
2
3
4
5
6
7
8
9
10
11
Month
Total AOD - NW Pacific
Dust AOD - NW Pacific
Total AOD - NE Pacific
Dust AOD - NE Pacific

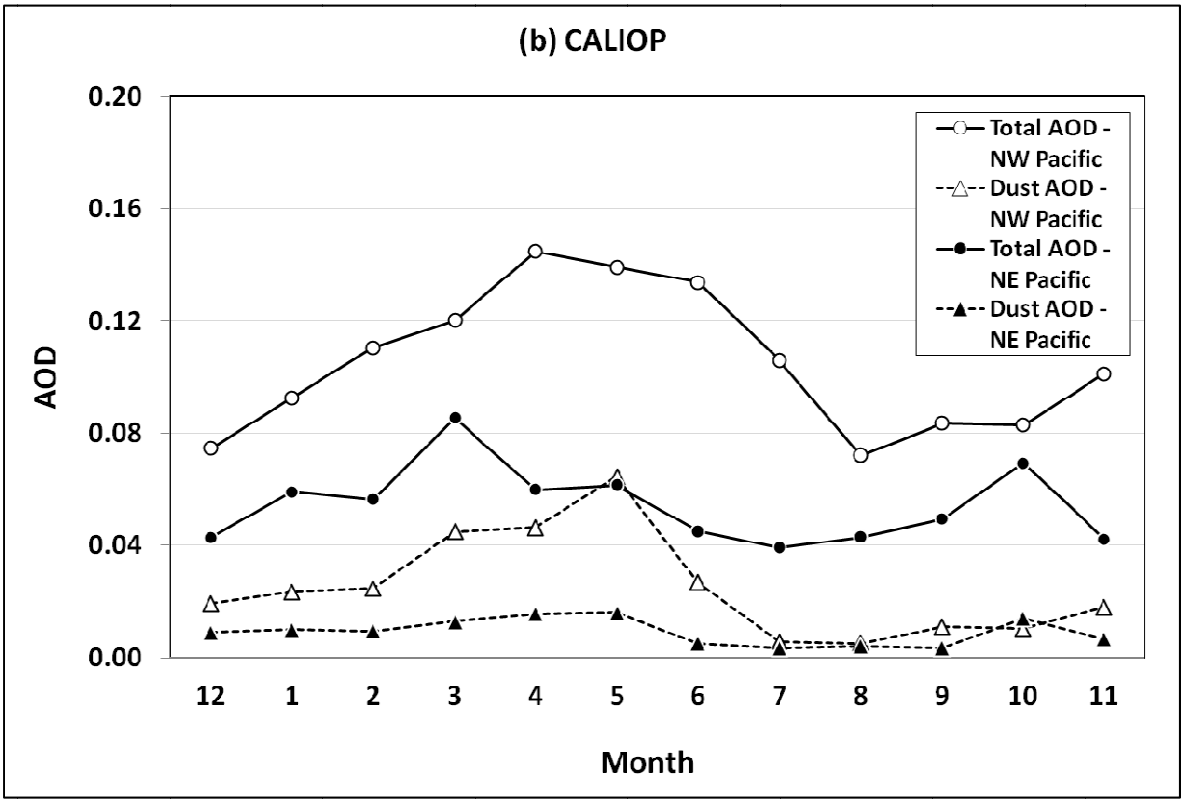
(b) CALIOP
AOD
0.20
0.16
0.12
0.08
0.04
0.00
12
1
2
3
4
5
6
7
8
9
10
11
Month
Total AOD - NW Pacific
Dust AOD - NW Pacific
Total AOD - NE Pacific
Dust AOD - NE Pacific

Appendix: Monthly MODIS Observations and Estimates

Table A.1 Monthly columnar AOD at 550 nm (AOD) observed by MODIS and the corresponding estimates of dust AOD (AOD_{du}), mass concentration (M_{du}), and eastward flux (F_{du}) for the East Asia outflow (a) and North America inflow (b) regions. u-wind is derived from the NCEP-Reanalysis 2 product.

(a)

Month	AOD	u-wind	AOD_{du}	M_{du} (g/m^2)	F_{du} (Tg)
12	0.246	11.1	0.106	0.288	45.2
1	0.256	11.7	0.098	0.266	45.2
2	0.283	11.9	0.100	0.271	35.9
3	0.365	9.4	0.162	0.436	71.3
4	0.473	8.41	0.310	0.837	115
5	0.513	6.43	0.352	0.95	71.1
6	0.325	4.63	0.140	0.377	23.6
7	0.309	4.20	0.101	0.273	16.4
8	0.212	3.32	0.090	0.242	8.22
9	0.187	4.91	0.092	0.247	15.5
10	0.202	7.56	0.092	0.248	21.1
11	0.213	10.2	0.0854	0.231	25.6

(b)

Month	AOD	u-wind	AOD_{du}	M_{du} (g/m^2)	F_{du} (Tg)
12	0.159	11.0	0.114	0.307	46.6
1	0.125	9.3	0.095	0.256	24.3
2	0.167	9.0	0.112	0.303	26.5
3	0.294	11.1	0.180	0.487	56.9
4	0.331	8.71	0.183	0.494	39.8
5	0.281	6.55	0.180	0.485	31.9
6	0.198	5.83	0.111	0.300	13.3
7	0.165	4.64	0.0777	0.210	4.39
8	0.112	4.20	0.0602	0.162	6.32
9	0.157	5.55	0.0818	0.221	14.0
10	0.156	9.3	0.105	0.283	26.0
11	0.138	8.87	0.094	0.254	28.5

Table A.2 Monthly columnar AOD at 532 nm (AOD) observed by CALIOP and the corresponding estimates of dust AOD (AOD_{du}), mass concentration (M_{du}), and eastward flux (F_{du}) for the East Asia outflow (a) and North America inflow (b) regions. u-wind is derived from the NCEP-Reanalysis 2 product.

(a)

Month	AOD	u-wind	AOD_{du}	M_{du} (g/m^2)	F_{du} (Tg)
12	0.0745	10.9	0.0192	0.0518	6.13
1	0.093	11.7	0.0234	0.0632	9.5
2	0.110	11.8	0.0245	0.0664	7.93
3	0.120	9.4	0.0449	0.121	19.4
4	0.145	8.54	0.0464	0.125	20.8
5	0.139	6.67	0.0645	0.174	18.7
6	0.134	4.56	0.0268	0.0723	6.19
7	0.106	4.64	0.00574	0.0155	1.08
8	0.0720	3.18	0.00501	0.0135	0.338
9	0.0835	5.13	0.0109	0.0293	2.87
10	0.0829	7.57	0.0104	0.0279	2.88
11	0.101	10.4	0.0179	0.0484	8.59

(b)

Month	AOD	u-wind	AOD_{du}	M_{du} (g/m^2)	F_{du} (Tg)
12	0.0428	10.6	0.0091	0.0245	2.5
1	0.0591	10.0	0.0099	0.0268	3.6
2	0.0563	9.1	0.0094	0.0255	1.8
3	0.0854	11.1	0.0128	0.0347	3.2
4	0.0599	8.64	0.0156	0.0421	3.3
5	0.0615	7.10	0.0160	0.0433	2.9
6	0.0451	5.92	0.00504	0.0136	0.3
7	0.0392	5.22	0.00338	0.0091	0.3
8	0.0429	4.30	0.00409	0.0110	0.4
9	0.0494	5.64	0.00338	0.0091	0.52
10	0.0692	9.4	0.0140	0.0379	2.6
11	0.042	8.72	0.00664	0.0179	1.5